Available online at www.sciencedirect.com

ScienceDirect

www.elsevier.com/locate/jes

JES JOURNAL OF ENVIRONMENTAL SCIENCES

www.jesc.ac.cn

A database of modeled gridded dry deposition velocities for 45 gaseous species and three particle size ranges across North America

Leiming Zhang[1,*], *Zhuanshi He*[1], *Zhiyong Wu*[1], *Anne Marie Macdonald*[1], *Jeffrey R. Brook*[1,2], *Shailesh Kharol*[1]

[1] *Air Quality Research Division, Science and Technology Branch, Environment and Climate Change Canada, Toronto, ON M3H 5T4, Canada*

[2] *Department of Chemical Engineering and Applied Chemistry, University of Toronto, Toronto, ON M5S 2E4, Canada*

ARTICLE INFO

Article history:
Received 8 February 2022
Revised 18 April 2022
Accepted 18 May 2022
Available online 29 May 2022

Keywords:
Air quality modeling
Atmospheric pollutant
Atmospheric deposition
Dry deposition velocity
Spatiotemporal distribution

ABSTRACT

The dry deposition process refers to the flux loss of an atmospheric pollutant due to uptake of the pollutant by the earth's surfaces. Dry deposition flux of a chemical species is typically calculated as the product of its surface-layer concentration and its dry deposition velocity (V_d). Field measurement based V_d data are very scarce or do not exist for many chemical species considered in chemistry transport models. In the present study, gaseous and particulate dry deposition schemes were applied to generate a database of hourly V_d for 45 gaseous species and three particle size ranges for two years (2016–2017) at a 15 km by 15 km horizontal resolution across North America. Hourly V_d of the 45 gaseous species ranged from < 0.001 to 4.6 cm/sec across the whole domain, with chemical species-dependent median (mean) values being in the range of 0.018–1.37 cm/sec (0.05–1.43 cm/sec). The spatial distributions of the two-year average V_d showed values higher than 1–3 cm/sec for those soluble and reactive species over certain land types. Soluble species have the highest V_d over water surfaces, while insoluble but reactive species have the highest V_d over forests. Hourly V_d of $PM_{2.5}$ across the whole domain ranged from 0.039 to 0.75 cm/sec with median (mean) value of 0.18 (0.20) cm s^{-1}, while the mean V_d for $PM_{2.5–10}$ is twice that of $PM_{2.5}$. Uncertainties in the modeled V_d are typically on the order of a factor of 2.0 or larger, which needs to be considered when applying the dataset in other studies.

Introduction

Atmospheric pollutants have important impacts on air quality and climate related issues such as visibility, radiative forcing, and human and ecosystem health (Fiore et al., 2015; Mukherjee and Agrawal, 2017; Wright et al., 2018; Tainio et al., 2021). Their lifetime in air is governed by four major processes including emission, transport, transformation and deposition (Seinfeld and Pandis, 2006). Deposition processes are the only pathway ultimately removing pollutants from the atmosphere and controls pollutants input into ecosystems. Emission pro-

* Corresponding author.
E-mail: leiming.zhang@ec.gc.ca (L. Zhang).

https://doi.org/10.1016/j.jes.2022.05.030

cesses release pollutants into the atmosphere, transport processes disperse pollutants around in the atmosphere, and transformation processes convert pollutants between different physical states and chemical forms. Excluding direct cloud droplet interception at high elevations or in fog, deposition can be divided into two sub-processes including dry and wet deposition. In dry deposition, gaseous or particulate pollutants are transported to the Earth's surface (e.g., vegetation, soil, water, snow, ice), where they become adsorbed. This is a slow and highly variable, but continuous process happening all the time and over any surface type. In wet deposition, pollutants are first scavenged by hydrometeors and then delivered to the Earth's surface through precipitation (e.g., snow, rain). On a regional or global scale and on annual (or longer period) basis, dry and wet deposition are equally important, and their relative importance depends on pollutant species, underlying surface, and precipitation amount (Lamarque et al., 2013; Vet et al., 2014).

Atmospheric deposition of many different chemical pollutants can cause detrimental effects on sensitive ecosystems, and subsequently affect human health (Cape et al., 2003; Wright et al., 2018). Monitoring networks have thus been established worldwide to monitor atmospheric deposition of some key atmospheric pollutants. At any given location, wet deposition can be monitored through the collection of precipitation amount and subsequent laboratory analysis of precipitation chemistry (Amodio et al., 2014). Uncertainties in wet deposition measurements range from about 10% to a factor of 2 depending on the level of pollutants in the precipitation (Otoshi et al., 2001). Compared to wet deposition, measurement of dry deposition is expensive and technically challenging (Mohan, 2016; Wright et al., 2016). Alternatively, dry deposition of a pollutant is commonly estimated using the inferential method, where flux is calculated as a product of the species concentration in air and modeled dry deposition velocity (V_d). Uncertainties in dry deposition measurements or estimates are typically on the order of a factor of 2 or larger, even for commonly studied species such as ozone and sulfur and nitrogen species (Flechard et al., 2011; Wu et al., 2015; Wu et al., 2018).

Existing data for V_d generated from field measurements were based on the measurements of air-surface exchange fluxes of pollutants of interest, and such data were mostly collected for gaseous species with appreciable ambient concentrations (Fowler et al., 2009). For gaseous species with trace levels in air and most chemically-resolved particle species, surrogate surface and other simplified methods were used to roughly estimate deposition fluxes, e.g., see a review of available measurements for mercury (Wright et al., 2016), polycyclic aromatic compounds (Zhang et al., 2015) and trace elements (Mamun et al., 2020). Using these simplified methods, the measured fluxes may not represent the actual ones and thus pose additional uncertainties on dry deposition models developed based on these flux datasets. V_d data for many pollutants are scarce or do not exist (Nguyen et al., 2015). To fill this data gap, V_d for 45 gaseous chemical species that are of interest in chemistry transport models and for three particle size-ranges are calculated at a temporal resolution of 1 h and a spatial resolution of 15 km by 15 km across North America. This data set is expected to be useful for estimating dry deposition of chemical species where ambient concentrations are monitored, or for comparison with chemistry transport models using different dry deposition schemes to more fully assess uncertainty ranges in dry deposition estimates (Galmarini et al., 2021).

1. Methodology

The dry deposition scheme of Zhang et al. (2003) originally included 31 gaseous species, and was recently extended to include additional 14 gaseous species by Wu et al. (2021). In this scheme V_d of gaseous species is calculated as:

$$V_d(z) = (R_a(z) + R_b + R_c)^{-1}, \quad (1)$$

where, R_a is the aerodynamic resistance, R_b the quasi-laminar sub-layer resistance, R_c the surface resistance, and z the reference height above the vegetation. R_c is parameterized as:

$$\frac{1}{R_c} = \frac{1 - W_{st}}{R_s + R_m} + \frac{1}{R_{ns}}, \quad (2)$$

$$\frac{1}{R_{ns}} = \frac{1}{R_{ac} + R_g} + \frac{1}{R_{cut}}, \quad (3)$$

where, R_s is the canopy stomatal resistance, R_m the mesophyll resistance, R_{ns} the non-stomatal resistance including resistance for uptake by leaf cuticles (R_{cut}) and by soil or ground litter (R_g), R_{ac} in-canopy aerodynamic resistance, and W_{st} the fraction of stomatal blocking under wet conditions. R_{cut} and R_g for any chemical species are scaled to those of SO_2 and O_3 with two species (i)-dependent scaling parameters $\alpha(i)$ and $\beta(i)$:

$$\frac{1}{R_{cut/g}(i)} = \frac{\alpha(i)}{R_{cut/g}(SO_2)} + \frac{\beta(i)}{R_{cut/g}(O_3)}. \quad (4)$$

The selection of α and β values was based on both theoretical considerations and available field flux measurements. Specifically, initial α values were first given based on the relative magnitudes of the effective Henry's Law constant of all the chemical species and that of SO_2, and initial β values were first given based on the relative magnitudes of the oxidizing capacity of all the chemical species. The α and β values were then tuned to best match the available flux data for most chemical species, and eventually, chemical species with high solubility were assigned with larger α values while those with high reactivity were assigned with large β values. Larger α and/or β values would result in smaller R_{ns} and thus larger V_d. Details of the R_s related formulas were described in Zhang et al. (2002), R_{ns} related formulas in Zhang et al. (2003), and R_a and R_b formulas in Wu et al. (2018). This model has been extensively evaluated in literature through comparison with field flux data. Uncertainties in the modeled V_d and associated dominant factors can also be found in Wu et al. (2018, 2021). The list of the 45 gaseous species and several species-dependent model parameters that are needed for discussing V_d results below are provided in Table S1.

The dry deposition scheme of Zhang and He (2014) calculates V_d for three particle size-ranges, i.e., fine ($PM_{2.5}$), coarse ($PM_{2.5-10}$) and giant (PM_{10+}) particles, representing particles

having a diameter of ≤ 2.5, 2.5–10 and > 10 μm, respectively. In this scheme V_d of particles is calculated as:

$$V_d = V_g + \frac{1}{R_a + 1/V_{ds}} \quad (5)$$

where V_g is the gravitational settling velocity and values of 3.7×10^{-5}, 1.8×10^{-3} and 3.4×10^{-2} m/sec are used for $PM_{2.5}$, $PM_{2.5\text{-}10}$ and PM_{10+}, respectively; V_{ds} is surface deposition, and is parameterized as a function of friction velocity (u_*) for $PM_{2.5}$ and as a function of u_* and leaf area index (LAI) for $PM_{2.5\text{-}10}$ and PM_{10+}. Detailed formulas and empirical parameters for V_{ds} can be found in Zhang and He (2014).

These two dry deposition schemes mentioned above are run together to provide V_d for 45 gaseous species and $PM_{2.5}$, $PM_{2.5-10}$ and PM_{10+}. V_d for individual gaseous species was provided because each gaseous species has its unique physical and chemical properties which largely control its deposition process. These 45 gaseous species cover the majority of chemical species that are dry deposited and simulated in community air quality models. V_d for particles were only provided for three particle size ranges because size distribution is the dominant factor affecting particle V_d. For the many individual particle chemical species, their V_d can then be estimated by their mass fractions in these three size ranges, as explained in Zhang and He (2014). Example applications of fine/coarse mass fractions in V_d calculation are available for polycyclic aromatic compounds in Zhang et al. (2015), particulate-bound mercury in Zhang et al. (2016), and trace elements in Mamun et al. (2022).

In our previous project of mapping dry deposition of reactive nitrogen over North America, we have developed a land cover database at a grid resolution of 15 km by 15 km (Kharol et al., 2018). We thus chose to use the same grid resolution for the present study. In this database, land cover information was extracted from the MODerate resolution Imaging Spectroradiometer (MODIS) land cover type product (MCD12Q1), which was derived from Terra- and Aqua-MODIS data of global land cover at 500 m spatial resolution. Five different schemes for land cover classification are available in the database. The primary land cover scheme identifies 17 land cover classes defined by the International Geosphere Biosphere Programme (IGBP) through a supervised decision-tree classification method (Friedli et al., 2002). The MCD12Q1 data from 2009 to 2013 was used to generate average land cover fractions for our model grid. Within each model grid, V_d is calculated for any existing individual land cover, and is then aggregated into a grid-averaged V_d by weighting land cover fractions within the grid. The fraction of forests and agricultural lands in each grid box (15 km x 15 km) is shown in Fig. S1.

We used archived 8-day average LAI (MCD15A2, https://ladsweb.modaps.eosdis.nasa.gov/missions-and-measurements/products/MCD15A2/, Yang et al., 2006) values at 1 km x 1 km spatial resolution to update the default LAI values in Zhang et al. (2003). Each LAI grid can contain four land cover pixel/grid due to different spatial resolutions between LAI data and land cover data. Therefore, we only used LAI grids having just one land cover type (pure) to generate land cover-specific LAI values. The average LAI values for each land cover are generated using the pure LAI grids over North America.

Meteorological data used as model input for calculating V_d are extracted from the archived data produced by the project "Precipitation and Ground Surface Reanalysis (REQA)" (Gasset et al., 2021), which contain three major sources (Global Deterministic Reforecast System, Regional Deterministic Reforecast System and Regional Surface Assimilation System). The archived data has a horizontal grid resolution of 10 km by 10 km, and required model parameters (solar flux absorbed at surface, geopotential height, relative humidity, specific humidity, total cloud cover, surface pressure, quantity of precipitation, snow depth, air temperature, and wind speed) at the REQA's first and/or second levels (40–50 m) were interpolated into our model grid at a resolution of 15 km by 15 km.

2. Results

Modeled V_d data for eight representative chemical species, including SO_2, O_3, HNO_3, HCN, HDC_4, ISOPN, HMHP and $PM_{2.5}$, are discussed below. Other species were only briefly compared with these eight species. As mentioned above, SO_2 and O_3 are the two base species chosen for scaling non-stomatal resistance for all the other gaseous species, and thus, the temporal and spatial patterns of V_d of many chemical species are similar to those of SO_2 or O_3 or their combinations. HNO_3 is the gaseous species having the minimum surface resistance among all the gaseous species in the model (Huebert and Robert, 1985), and thus, its V_d basically represents the characteristics of surface types and meteorological conditions. These three species are among the list of gaseous species modeled in Zhang et al. (2003). The next four species are among the recently added ones to the model, as described in Wu et al. (2021). Among these four species, HCN is the only non-VOC species, and the three VOC species (HDC_4, ISOPN and HMHP) selected here represent those with relatively low, medium and high V_d values among all the VOCs considered in the model. The last one is $PM_{2.5}$, representing fine particles. For each of these eight species, statistics of hourly V_d over the whole domain and over forest and agricultural dominated grids were first provided, annual and seasonal average V_d maps were then discussed. To avoid misleading results from a few extremely small or large V_d values (which are very common from field measurement data, but less so from the modeled data), we choose to mainly focus on discussing the 5th–95th range and the median and mean value.

Statistics of the modeled hourly V_d for the 45 gaseous species and three particle size ranges across the whole domain are shown in Table 1, and those of the grids dominated by forests and agricultural lands are shown in Tables S2 and S3, respectively. Statistics of the modeled hourly V_d for the eight representative chemical species across the whole domain are also shown in Fig. 1. Maps of the two-year average V_d for these eight species are shown in Fig. 2, and a full set of the V_d maps of the 48 species (in the same sequence as in Table 1) are provided in Fig. S2. Seasonal average V_d for the eight species are shown in Fig. S3.

Table 1 – Statistics of the modeled hourly V_d (cm/sec) during a two-year (2016–2017) period over the North America domain. The seven column numbers are for domain-wide minimum (Min), 5th percentile, median (Med), mean, standard deviation (Std), 95th percentile, and maximum (Max) V_d values.

No.	Symbol	Name	Min	5th	Med	Mean	Std	95th	Max
1	SO_2	Sulphur dioxide	0.0010	0.0423	0.418	0.546	0.453	1.42	3.69
2	H_2SO_4	Sulphuric acid	0.0010	0.0481	0.497	0.605	0.478	1.51	4.37
3	NO_2	Nitrogen dioxide	0.0009	0.0210	0.136	0.202	0.179	0.57	2.22
4	O_3	Ozone	0.0009	0.0239	0.156	0.226	0.194	0.61	2.53
5	H_2O_2	Hydrogen peroxide	0.0013	0.0500	0.529	0.643	0.507	1.60	4.54
6	HNO_3	Nitric acid	0.0049	0.0751	1.375	1.431	0.980	3.23	4.60
7	HONO	Nitrous acid	0.0016	0.0605	0.746	0.873	0.690	2.21	4.60
8	HNO_4	Pernitric acid	0.0028	0.0693	1.080	1.184	0.869	2.90	4.57
9	NH_3	Ammonia	0.0014	0.0455	0.468	0.604	0.492	1.54	3.90
10	PAN	Peroxyacetylnitrate	0.0006	0.0172	0.106	0.154	0.133	0.42	1.73
11	PPN	Peroxypropylnitrate	0.0006	0.0172	0.105	0.152	0.130	0.41	1.72
12	APAN	Aromatic acylnitrate	0.0006	0.0203	0.124	0.174	0.144	0.45	2.05
13	MPAN	Peroxymethacrylic nitric anhydride	0.0005	0.0110	0.065	0.105	0.099	0.31	1.08
14	HCHO	Formaldehyde	0.0011	0.0423	0.423	0.535	0.430	1.35	3.62
15	MCHO	Acetaldehyde	0.0004	0.0034	0.020	0.065	0.090	0.27	0.56
16	PALD	C3 Carbonyls	0.0004	0.0033	0.020	0.061	0.083	0.25	0.54
17	C4A	C4-C5 Carbonyls	0.0004	0.0033	0.019	0.057	0.078	0.24	0.52
18	C7A	C6-C8 Carbonyls	0.0003	0.0032	0.018	0.050	0.066	0.20	0.46
19	ACHO	Aromatic carbonyls	0.0003	0.0032	0.019	0.052	0.070	0.21	0.48
20	MVK	Methyl-vinyl-ketone	0.0004	0.0033	0.019	0.070	0.106	0.31	1.00
21	MACR	Methacrolein	0.0004	0.0033	0.019	0.058	0.079	0.24	0.52
22	MGLY	Methylgloxal	0.0003	0.0034	0.020	0.069	0.104	0.31	0.98
23	MOH	Methyl alcohol	0.0011	0.0366	0.355	0.454	0.365	1.14	3.05
24	ETOH	Ethyl alcohol	0.0009	0.0353	0.333	0.433	0.352	1.10	2.87
25	POH	C3 alcohol	0.0008	0.0287	0.260	0.341	0.276	0.87	2.31
26	CRES	Cresol	0.0003	0.0033	0.020	0.062	0.090	0.27	0.85
27	FORM	Formic acid	0.0014	0.0566	0.654	0.799	0.651	2.08	4.60
28	ACAC	Acetic acid	0.0011	0.0508	0.537	0.680	0.558	1.77	4.46
29	ROOH	Organic peroxides	0.0009	0.0273	0.238	0.276	0.208	0.68	2.54
30	ONIT	Organic nitrates	0.0007	0.0155	0.096	0.138	0.118	0.37	1.51
31	INIT	Isoprene nitrate	0.0006	0.0153	0.092	0.130	0.108	0.34	1.47
32	HCN	Hydrogen cyanide	0.0006	0.0057	0.034	0.085	0.106	0.33	0.66
33	HMHP	Hydroxymethyl hydroperoxide	0.0022	0.0678	1.004	1.127	0.858	2.86	4.59
34	HAC	Hydroxyacetone	0.0012	0.0538	0.597	0.725	0.579	1.84	4.55
35	PAA	Peroxyacetic acid	0.0014	0.0573	0.681	0.811	0.650	2.08	4.55
36	HDC_4	The C4 hydroxy dicarbonyl from IEPOX oxidation	0.0009	0.0443	0.436	0.554	0.450	1.42	3.80
37	DHC_4	The C4 dihydroxy carbonyl from IEPOX oxidation	0.0012	0.0546	0.628	0.762	0.621	1.99	4.51
38	HPALD	Isoprene hydroperoxy aldehydes	0.0011	0.0527	0.584	0.706	0.565	1.80	4.49
39	ISOPOOH	Isoprene hydroxyhydroperoxide	0.0020	0.0651	0.947	1.067	0.816	2.72	4.52
40	IEPOX	Isoprene dihydroxyepoxide	0.0020	0.0651	0.947	1.067	0.816	2.72	4.52
41	PROPNN	Propanone nitrate or propanal nitrate	0.0011	0.0526	0.583	0.705	0.564	1.80	4.49
42	ISOPN	Isoprene hydroxy nitrates	0.0011	0.0521	0.577	0.697	0.557	1.77	4.46
43	MACN/MVKN	Methacrolein and Methyl vinyl ketone hydroxy nitrate	0.0011	0.0521	0.576	0.696	0.556	1.77	4.46
44	INP	Isoprene nitrooxy hydroperoxide	0.0011	0.0518	0.573	0.693	0.553	1.76	4.45
45	MTNP	Monoterpene nitrooxy hydroperoxide	0.0010	0.0509	0.563	0.678	0.541	1.73	4.40
1	$PM_{2.5}$	Fine particles	0.0338	0.0393	0.177	0.199	0.131	0.45	0.94
2	$PM_{2.5-10}$	Coarse particles	0.1847	0.1885	0.253	0.396	0.360	1.10	7.12
3	PM_{10+}	Giant particles	3.4758	3.5309	5.402	6.243	2.569	11.11	13.21

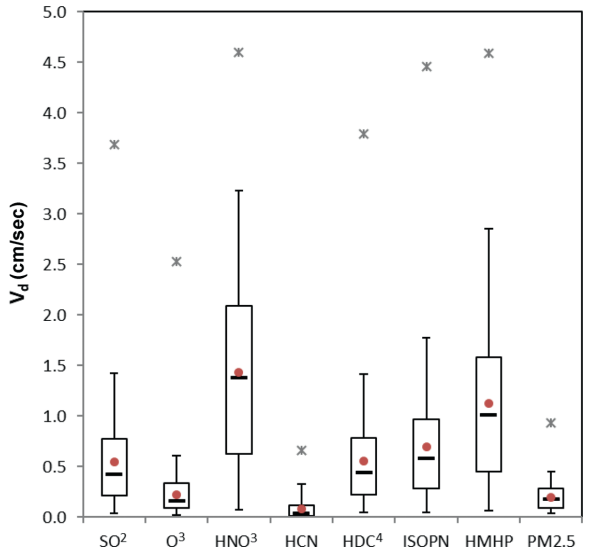

Fig. 1 – Statistics of hourly V_d for the eight representative chemical species across the whole model domain. The box and whisker represent the central 50% (25th–75th percentile) and 90% (5th and 95th) data, respectively. Short horizontal line, solid circle and star symbol represent median, mean and maximum V_d values, respectively.

2.1. *SO_2 and O_3*

The 5th–95th range of the hourly V_d for SO_2 are 0.04–1.4 cm/sec across the whole model domain, 0.04–1.8 cm/sec over forests, and 0.05–1.2 cm/sec over agricultural lands, and the median (mean) values are 0.42 (0.55), 0.43 (0.58) and 0.51(0.56) cm/sec, respectively. The 5th–95th range of the hourly V_d for O_3 are 0.02–0.61 cm/sec across the whole model domain, 0.02–0.75 cm/sec over forests, and 0.03–0.56 cm/sec over agricultural lands, and the median (mean) values are 0.16 (0.23), 0.25 (0.31) and 0.13(0.21) cm/sec[1], respectively. The smallest V_d values were mostly for nighttime periods when leaf stoma are generally closed and the atmospheric surface layer is in stable condition.

The above statistical V_d values demonstrate that SO_2 and O_3 behave quite differently in terms of dry deposition process. For example, the median (mean) V_d are much higher over forests than agricultural lands for O_3, but are quite close for SO_2. Besides, V_d are much higher for SO_2 than O_3 over most surfaces. Stomatal and non-stomatal uptake contribute equally to O_3 V_d on an annual basis (Zhang et al., 2006), and O_3 V_d does not differ much between dry and wet surfaces (Zhang et al., 2002). This explains the higher O_3 V_d over forests than agricultural lands due to the higher leaf area index of the former than the latter land cover type. In contrast, SO_2 V_d is much higher over wet and humid than dry surface, which can cause the much higher contribution from non-stomatal than stomatal uptake in areas under wet and/or humid conditions. Because O_3 has a smaller molecular weight (larger molecular diffusivity) than SO_2, the stomatal uptake is actually slightly higher for O_3 than SO_2. Thus, the higher V_d for SO_2 than O_3 over vegetated surfaces is due to the much higher nonstomatal uptake of SO_2.

Another reason for the wide range of SO_2 V_d across the whole domain is because of some ocean surfaces covered by the model domain. As can be seen from Fig. 2, the highest annual average SO_2 V_d (> 1 cm/sec) appears over ocean surfaces. Annual average SO_2 V_d is also quite high (0.5–1.0 cm/sec) over most forests and agricultural lands. O_3 V_d showed a different pattern than that of SO_2 V_d, no just over water surface, but also over agricultural lands. The similarities between SO_2 and O_3 V_d lie over forests, where both SO_2 and O_3 showed high values in the forest regions in southeastern U.S. and a large part of Canada.

Both SO_2 and O_3 show highest V_d in summer and lowest in winter over vegetated surfaces in mid to high latitude regions due to the seasonal variations of LAI (Fig. S3). Seasonal variations of V_d are small in low latitude regions due to the year-round warm temperatures.

Chemical species with the scaling parameter "α" being set to 0 (or $\beta >> \alpha$) should behave similarly to O_3 to certain extent, while those with the scaling parameter "β" being set to 0 (or $\alpha >> \beta$) should behave similarly to SO_2 (see Table S1 α and β values for each species). For example, the spatial pattern of NH_3 V_d ($\alpha = 1$ and $\beta = 0$) is basically the same as that of SO_2 (Fig. S2) except with slightly higher values. The higher V_d for NH_3 than SO_2 (by approximately 10%) is due to the faster stomatal uptake of NH_3 due to its smaller molecular weight. Other species that have similar V_d spatiotemporal patterns to those of SO_2 include MOH, ETOH, POH, FORM and ACAC (see Table 1 for definitions) with the former three having lower V_d (by 20%–30%) and the latter two having higher V_d (by > 30%) than that of SO_2. Similarly, species that have similar V_d spatiotemporal patterns to those of O_3 include NO_2, PAN, PPN, APAN, MPAN, ROOH, ONIT and INIT (Table 1), but with lower V_d than that of O_3. Domain-wide mean V_d values were 10–50% lower for these species than O_3. For the rest of the first 31 chemical species listed in Table S1, α and β values are either comparable or both are extremely small (e.g., < 0.1). In the former case, the spatial pattern of V_d of the chemical species would show a combined feature from both SO_2 and O_3. In the latter case nonstomatal uptake becomes very small or even negligible and V_d pattern is mainly dominated by LAI distribution.

2.2. *HNO_3*

Hourly V_d for HNO_3 across the whole model domain is in the range of 0.005–4.6 cm/sec, and the 5th–95th range is 0.08–3.2 cm/sec (Table 1). The median and mean V_d values are both around 1.4 cm/sec. The median and mean V_d values are 2%–6% lower over agricultural lands and 20% higher over forests than those over the whole domain (Tables S2 and S3), which are likely caused by different roughness length over different surfaces. Surface resistance for HNO_3 is expected to be very small (Huebert and Robert, 1985), and the smallest V_d values were thus due to extreme stable conditions in the atmospheric surface layer, which resulted in very large aerodynamic resistance. The two scaling parameters ($\alpha = 10$ and $\beta = 10$) assigned to HNO_3 would give it a surface resistance being on the order of 5–10% of those of SO_2. If setting a zero surface resistance for HNO_3, as is done in some dry depositions schemes, V_d would

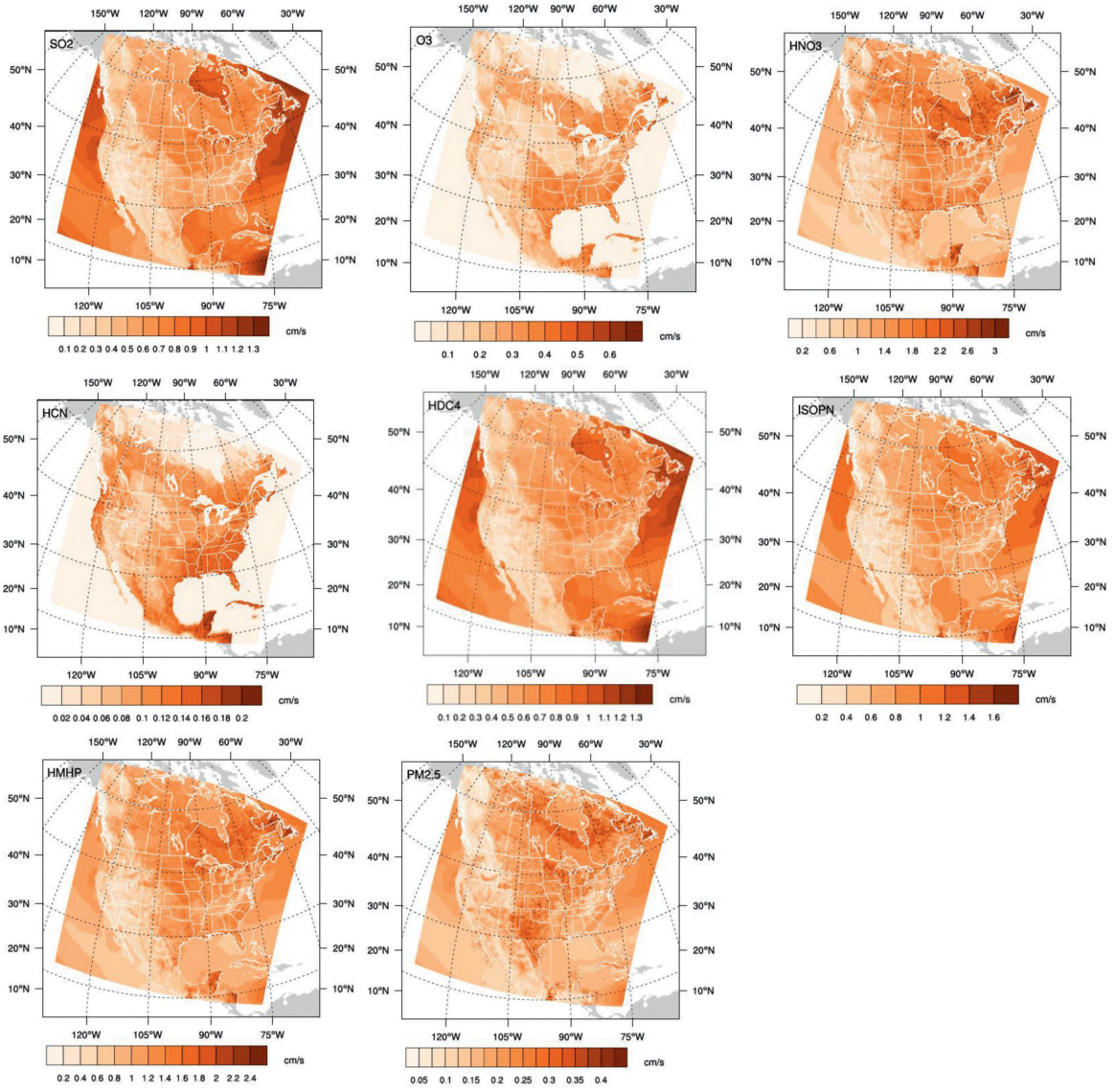

Fig. 2 – Maps of the two-year average V_d for the eight representative chemical species.

only be increased by a small percentage under most conditions (e.g., for V_d lower than our 90th percentile), but can increase V_d by up to 50% for the V_d values in the upper part of the distribution.

Comparing the spatial distributions between the annual average V_d (Fig. 2) and land cover of forests and agricultural lands (Fig. S1), it can be seen that the highest V_d do not always appear over forest areas, implying meteorological conditions, besides roughness length, also play an important role on HNO_3 deposition because aerodynamic resistance generally dominates HNO_3 V_d. In fact, meteorological conditions, especially wind speed and surface layer stratification, all of which affect atmospheric turbulence, are the dominant factors controlling HNO_3 V_d. Seasonal variations of HNO_3 V_d are not as large as those for SO_2 and O_3, although HNO_3 V_d seem to be slightly higher in summer and fall than in spring and winter in eastern half of Canada (Fig. S3).

V_d of HNO_2 and HNO_4 might be as high as that of HNO_3 in reality, but were assumed to have somewhat lower V_d than HNO_3 V_d in the model (i.e., $\alpha = \beta = 2$ for HNO_2 and $\alpha = \beta = 5$ for HNO_4). Domain-wide mean V_d are 40% and 20% smaller for HNO_2 and HNO_4, compared to HNO_3, respectively. H_2SO_4 and H_2O_2 are also very soluble and reactive ($\alpha = \beta = 1$ for both species), and their V_d are about 55-60% lower than that of HNO_3 in terms of domain wide average).

2.3. *HCN*

The 5th–95th range of the hourly V_d for HCN are 0.006–0.33 cm/sec across the whole model domain, and the median and mean values are 0.034 and 0.085, respectively, (Fig. 2). The 5th–95th range does not differ much over forests and agricultural lands, but the median and mean values are indeed higher over forests (0.052 and 0.12) than over agricultural lands (0.031 and 0.083). This is because non-stomatal uptake is not important for HCN (with $\alpha = 0$ and $\beta = 0.1$) and the stom-

atal uptake (and thus LAI) controls V_d. Due to the same reason, HCN V_d is the highest in summer when LAI is the largest, followed by spring and autumn, and the lowest in winter, and the seasonal variations are much larger in high latitudes than low latitudes (Fig. S3).

2.4. *VOCs*

All the VOCs considered in the model are soluble (α = 1.5-5) and most of these VOCs are quite reactive (β = 0.2 for four species and β = 1 for the rest of the species) (Fig. S1). The high α and β values given for these species warrant the dominant contribution from non-stomatal uptake to the total V_d, especially with the decreasing contribution from stomatal uptake due to the very high molecular weight (small molecular diffusivity) of some of the VOCs. The molecular weight of these VOCs are in the range of 64-231 (Table S1).

HDC_4, ISOPN and HMHP can represent those VOCs with relatively low, medium and high V_d values, respectively. The 5th–95th range of the hourly V_d for HDC_4 are 0.04–1.4 cm/sec across the whole model domain, 0.04–1.8 cm/sec over forests, and 0.05–1.2 cm/sec over agricultural lands, and the median (mean) values are 0.44 (0.55), 0.43 (0.58) and 0.52(0.56) cm/sec, respectively. The 5th–95th range of the hourly V_d for ISOPN are 0.05–1.8 cm/sec across the whole model domain, 0.05–2.3 cm/sec over forests, and 0.05–1.5 cm/sec over agricultural lands, and the median (mean) values are 0.58 (0.70), 0.57 (0.75) and 0.65(0.70) cm/sec, respectively. The 5th–95th range of the hourly V_d for HMHP are 0.07–2.9 cm/sec across the whole model domain, 0.07–3.6 cm/sec over forests, and 0.07–2.4 cm/sec over agricultural lands, and the median (mean) values are 1.0 (1.1), 1.1 (1.3) and 1.1(1.1) cm/sec, respectively. The maximum V_d values for these three species are 3.8, 4.5 and 4.6 cm/sec, respectively, the latter two values being very close to that of HNO_3. Due to the high solubility of these VOC species, V_d is much higher over wet and humid than dry surfaces, similar to the case for SO_2 discussed above. This explains the insignificant difference in V_d between forests and agricultural lands.

Spatial distributions and seasonal variations of HDC_4 V_d are similar to those of SO_2 V_d to a large extent (Figs. 2 and S3), and their domain-wide mean V_d are also very close, which can be explained largely by the assigned α (= 1.0) and β (= 0.2) values for HDC_4. Spatial distributions and seasonal variations of ISOPN V_d (α = 1.5 and β = 1.0) are also similar to those of SO_2 V_d to some extent, but with nearly 30% higher V_d in terms of domain-wide average. Spatial distributions of HMHP V_d (α = 5.0 and β = 1.0) are similar to those of HNO_3 V_d to a large extent, although with slightly lower values (by 20% in terms of domain wide mean value).

ISOPOOH and IEPOX, both of which are assigned an α value of 5.0, will have similar spatiotemporal distributions to those of HMHP. Most of the other VOCs species will have similar spatiotemporal distributions to those of ISOPN.

2.5. *Particles*

The 5th–95th range of the hourly V_d for $PM_{2.5}$ are 0.04–0.45 cm/sec across the whole model domain, and the median and mean V_d are 0.18 and 0.20 cm/sec, respectively. The statistical numbers of V_d do not differ significantly between forests and agricultural lands, which is somewhat in contrast to available field data that shows higher V_d over forests. This finding is similar to the case of HNO_3 discussed above, which is attributed to different metrological conditions in different regions. The spatiotemporal pattern of $PM_{2.5}$ V_d and HNO_3 V_d indeed have a certain degree of similarity (Fig. 2) if excluding ocean surfaces, e.g., with higher values over most forests and agricultural lands than other land areas.

Domain-wide median V_d for $PM_{2.5\text{-}10}$ is 40% higher than that of $PM_{2.5}$, but mean V_d doubled. Domain-wide mean and median V_d for PM_{10+} are both higher than 5 cm/sec. The relative standard deviation is 65%, 90% and 40% for the mean V_d of $PM_{2.5}$, $PM_{2.5\text{-}10}$ and PM_{10+}, respectively, implying a much smaller variation for PM_{10+} than for smaller particles due to the dominance of gravitational setting on PM_{10+} V_d. Note that in some literature, V_d of $PM_{2.5\text{-}10}$ is assumed to be much large than that of V_d of $PM_{2.5}$. This is because many size-resolved particle V_d models, especially those developed in early years, give very low V_d for particles smaller than 1 μm. Zhang et al. (2001) realized the much higher V_d values obtained from field measurements conducted in later 1990's, and constructed the model to produce higher V_d for fine particles. Based on the size-resolved model of Zhang et al. (2001), Zhang and He (2014) then developed a bulk version of the particle V_d model for $PM_{2.5}$, $PM_{2.5\text{-}10}$ and PM_{10+}, which is the one used in the present study. Khan and Perlinger (2017) also reported that the Zhang and He (2014) model produces better results for V_d of fine particles than other models. Thus, the differences in V_d between $PM_{2.5}$ and $PM_{2.5\text{-}10}$ in the present study was not as large as traditionally assumed in literature.

Seasonal variations of $PM_{2.5}$ V_d are small (Fig. S3). Note that LAI is indeed a parameter implicitly considered in calculating $PM_{2.5}$ V_d and explicitly included in the V_d formulation for $PM_{2.5\text{-}10}$ and PM_{10+} V_d. Larger LAI gives high V_d for some canopies with changing LAI (e.g., deciduous forest and most agricultural lands). Seasonal variations of $PM_{2.5\text{-}10}$ are larger than those of $PM_{2.5}$, as is also supported by the much larger standard deviation mentioned above (Figure not shown). Seasonal variations of PM_{10+} are small due to the same reason mentioned above.

3. Summary

A database of hourly V_d for 45 gaseous species and three particle size ranges at 15 km by 15 km horizontal resolution across North America was developed using community dry deposition schemes, reanalyzed forecasted meteorology and satellite generated land cover and leaf area index data. Statistics of the hourly V_d and annual and seasonal average V_d for eight representative chemical species over the whole domain and over forest and agricultural lands were discussed in detail. V_d of the other chemical species were briefly compared to these representative species. Based on earlier evaluations and intercomparisons of the dry deposition schemes (e.g., Wu et al. 2018) used in the present study, we believe that V_d for inorganic gaseous species shown here are in reasonable and medium range compared to available flux measurement data and V_d

produced by the other existing schemes. Daytime V_d for some VOCs (e.g., HMHP, HAC, PAA, HPALD, PROPPN) might be conservative estimates when compared to the very limited field data, as shown in Wu et al. (2021). The uncertainties as large as a factor of 2.0, even on seasonal to annual time scales, in modeled V_d data need to be taken into account when applying the data set in ecosystem impact studies concerning various pollutants.

Appendix A Supplementary data

Supplementary material associated with this article can be found, in the online version, at doi:10.1016/j.jes.2022.05.030. The computer code and data used in this study can be obtained by contacting the corresponding author. The code is also available from (DOI:10.5281/zenodo.4697426): https://zenodo.org/record/4697426#.YHmzu5-Sk2w.

REFERENCES

Amodio, M., Catino, S., Dambruoso, P., De Gennaro, G., Di Gilio, A., Giungato, P., et al., 2014. Atmospheric deposition: sampling procedures, analytical methods, and main recent findings from the scientific literature. Adv. Meteorol. 2014, 161730.

Cape, J.N., Fowler, D., Davison, A., 2003. Ecological effects of sulfur dioxide, fluorides, and minor air pollutants: recent trends and research needs. Environ. Int. 29 (2-3), 201–211.

Fiore, A.M., Naik, V., Leibensperger, E.M., 2015. Air quality and climate connections. J. Air Waste Manag. 65 (6), 645–685.

Flechard, C., Nemitz, E., Smith, R., Fowler, D., Vermeulen, A., Bleeker, A., et al., 2011. Dry deposition of reactive nitrogen to European ecosystems: a comparison of inferential models across the NitroEurope network. Atmos. Chem. Phys. 11 (6), 2703–2728.

Fowler, D., Pilegaard, K., Sutton, M.A., Ambus, P., Raivonen, M., Duyzer, J., et al., 2009. Atmospheric composition change: ecosystems-atmosphere interactions. Atmos. Environ. 43 (33), 5193–5267.

Friedli, M.A., McIver, D.K., Hodges, J.C., Zhang, X.Y., Muchoney, D., Strahler, A.H., et al., 2002. Global land cover mapping from MODIS: algorithms and early results. Remote Sensing of Environment 83, 287–302.

Galmarini, S., Makar, P., Clifton, O.E., Hogrefe, C., Bash, J.O., Bellasio, R., et al., 2021. Technical note: AQMEII4 activity 1: evaluation of wet and dry deposition schemes as an integral part of regional-scale air quality models. Atmos. Chem. Phys. 21, 15663–15697.

Gasset, N., Fortin, V., Dimitrijevic, M., Carrera, M., Bilodeau, B., Muncaster, R., et al., 2021. A 10 km North American precipitation and land-surface reanalysis based on the GEM atmospheric model. Hydrol. Earth Syst. Sci. 25, 4917–4945.

Khan, T.R., Perlinger, J.A., 2017. Evaluation of five dry particle deposition parameterizations for incorporation into atmospheric transport models. Geosci. Model Dev. 10, 3861–3888.

Kharol, S.K., Shephard, M.W., Mclinden, C.A., Zhang, L., Sioris, C.E., O'Brien, J.O., et al., 2018. Dry deposition of reactive nitrogen from satellite observations of ammonia and nitrogen dioxide over North America. Geophys. Res. Lett. 45, 1157–1166.

Lamarque, J.F., Dentener, F., McConnell, J., Ro, C.U., Shaw, M., Vet, R., et al., 2013. Multi-model mean nitrogen and sulfur deposition from the atmospheric chemistry and climate model intercomparison project (ACCMIP): evaluation historical and projected changes. Atmos. Chem. Phys. 13 (16), 7997–8018.

Mohan, S.M., 2016. An overview of particulate dry deposition: measuring methods, deposition velocity and controlling factors. Int. J. Environ. Sci. Technol. 13 (1), 387–402.

Mamun, A.A., Cheng, I., Zhang, L., Dabek-Zlotorzynska, E., Charland, J.P., 2020. Overview of size distribution, concentration, and dry deposition of airborne particulate elements measured worldwide. Environ. Rev. 28, 77–88.

Mamun, A.A., Cheng, I., Zhang, L., Celo, V., Dabek-Zlotorzynska, E., Charland, J.P., 2022. Estimation of atmospheric dry and wet deposition of particulate elements at four monitoring sites in the Canadian Athabasca oil sands region. J. Geophys. Res. Atmos. 127, e2021JD035787.

Mukherjee, A., Agrawal, M., 2017. World air particulate matter: sources, distribution and health effects. Environ. Chem. Lett. 15 (2), 283–309.

Seinfeld, J., Pandis, S., 2006. Atmospheric Chemistry and Physics: from Air Pollution to Climate Change. John Wiley & Sons Book.

Nguyen, T.B., Crounse, J.D., Teng, A.P., Clair, J.M.S., Paulot, F., Wolfe, G.M., et al., 2015. Rapid deposition of oxidized biogenic compounds to a temperate forest. Proceedings of the National Academy of Sciences 112, E392–E401.

Otoshi, T., Fukuzaki, N., Li, H., Hoshino, H., Sase, H., Saito, M., Suzuki, K., 2001. Quality control and its constraints during the preparatory-phase activities of the acid deposition monitoring network in East Asia (EANET). Water Air Soil Pollut. 130, 1613–1618.

Tainio, M., Jovanovic Andersen, Z., Nieuwenhuijsen, M.J., Hu, L., de Nazelle, A., An, R., et al., 2021. Air pollution, physical activity and health: a mapping review of the evidence. Environ. Int. 147, 105954.

Vet, R., Artz, R.S., Carou, S., Shaw, M., Ro, C.U., Aas, W., et al., 2014. A global assessment of precipitation chemistry and deposition of sulfur, nitrogen, sea salt, base cations, organic acids, acidity and pH, and phosphorus. Atmos. Environ. 93, 3–100.

Wright, L.P., Zhang, L., Marsik, F.J., 2016. Overview of mercury dry deposition, litterfall, and throughfall studies. Atmos. Chem. Phys. 16 (21), 13399–13416.

Wright, L.P., Zhang, L., Cheng, I., Aherne, J., Wentworth, G.R., 2018. Impacts and effects indicators of atmospheric deposition of major pollutants to various ecosystems-a review. Aerosol Air Qual. Res. 18, 1953–1992.

Wu, Z.Y., Zhang, L., Wang, X.M., Munger, J.W., 2015. A modified micrometeorological gradient method for estimating O_3 dry depositions over a forest canopy. Atmos. Chem. Phys. 15 (13), 7487–7496.

Wu, Z.Y., Schwede, D.B., Vet, R., Walker, J.T., Shaw, M., Staebler, R., Zhang, L., 2018. Evaluation and intercomparison of five North American dry deposition algorithms at a mixed forest site. J. Adv. Model. Earth Syst. 10, 1571–1586.

Wu, Z., Zhang, L., Walker, J.T., Makar, P.A., Perlinger, J.A, Wang, X., 2021. Extension of a gaseous dry deposition algorithm to oxidized volatile organic compounds and hydrogen cyanide for application in chemistry transport models. Geosci. Model Dev. 14, 5093–5105.

Yang, W., Tan, B., Huang, D., Rautiainen, M., Shabanov, N.V., Wang, Y., et al., 2006. MODIS leaf area index products: From validation to algorithm improvement. IEEE Transactions on Geoscience and Remote Sensing 44 (7), 1885–1896.

Zhang, L., Brook, J.R., Vet, R., 2002. On ozone dry deposition –with emphasis on non-stomatal uptake and wet canopies. Atmos. Environ. 36, 4787–4799.

Zhang, L., Brook, J., Vet, R., 2003. A revised parameterization for gaseous dry deposition in air-quality models. Atmos. Chem. Phys. 3, 2067–2082.

Zhang, L., Vet, R., Brook, J.R., Legge, A.H., 2006. Factors affecting stomatal uptake of ozone by different canopies and a

comparison between dose and exposure. Sci. Total Environ. 370, 117–132.
Zhang, L., Gong, S., Padro, J., Barrie, L.A., 2001. A size-segregated particle dry deposition scheme for an atmospheric aerosol module. Atmospheric Environment 35, 549–560.
Zhang, L., He, Z., 2014. Technical note: an empirical algorithm estimating dry deposition velocity of fine, coarse and giant particles. Atmos. Chem. Phys. 14, 3729–3737.
Zhang, L., Cheng, I., Wu, Z., Harner, T., Schuster, J., Charland, J.P., et al., 2015. Dry deposition of polycyclic aromatic compounds to various land covers in the Athabasca oil sands region. J. Adv. Model. Earth Syst. 7, 1339–1350.
Zhang, L., Wu, Z., Cheng, I., Wright, L.P, Olson, M.L., Gay, D.A, et al., 2016. The estimated six-year mercury dry deposition across North America. Environ. Sci. Technol. 50, 12864–12873.